

MODEL-BASED SEGMENTATION OF CARDIAC AND VASCULAR IMAGES

W. J. Niessen, C. M. van Bommel, A. F. Frangi, M. J. A. Siers, O. Wink

Image Sciences Institute, University Medical Center Utrecht
Room E.01.334, Heidelberglaan 100, 3584 CX Utrecht, The Netherlands; wiro@isi.uu.nl

ABSTRACT

Model-based approaches towards the segmentation of vascular and cardiac images are presented. For vessel segmentation, prior shape information is introduced based on the notion that vessels are elongated structures. For cardiac segmentation, shape information derived from a training set of segmented images is incorporated in an automatically constructed point distribution model of the heart.

1. INTRODUCTION

In order to improve accuracy and robustness of medical image segmentation, model- or knowledge based approaches have become increasingly popular. Whereas prior knowledge may concern knowledge of the image formation process, or information of the medical expert interpreting the image, most emphasis in model-based segmentation has been put on constraining the shape of the objects to be segmented. The most commonly used approach, including the large body of work on deformable models [1, 2], includes a smoothness term in order to enforce regularity of the object contour or surface. Other approaches explicitly limit the space of possible shapes. For an overview of these approaches applied to cardiac image segmentation we refer to a recent review article by Frangi et al. [3].

In this paper, some of our work on model-based segmentation of cardiac, vascular, and cardiovascular images is described. In case of vessel segmentation and quantification, the a priori knowledge that the object is an elongated structure is used. In cardiac segmentation, a point distribution model of the heart for active shape model (ASM) segmentation is automatically constructed from a set of segmented training shapes using volumetric elastic registration.

2. VASCULAR IMAGE PROCESSING

Vessel segmentation and quantification has received considerable interest, see *e.g.* [4-9]. The approach which is adopted in the majority of our work [10-15] is based on a two step approach. First, centerline(s) of a vessel segment or vessel network are obtained, prior to quantification, visualization or segmentation.

In order to extract the vessel axis, a feature image is constructed which determines the likeliness that a voxel belongs to (the center of) the vessel. This likeliness is defined as a discriminant function [16] based on the eigenvalues $|\lambda_1| \leq |\lambda_2| \leq |\lambda_3|$ of the Hessian matrix:

$$\mathcal{V} = \begin{cases} 0 & \text{if } \lambda_2 > 0 \text{ or } \lambda_3 > 0, \\ \left[1 - \exp\left(-\frac{\mathcal{R}_A^2}{2\alpha^2}\right)\right] \exp\left(-\frac{\mathcal{R}_B^2}{2\beta^2}\right) \left[1 - \exp\left(-\frac{\mathcal{S}^2}{2c^2}\right)\right] & \end{cases} \quad (1)$$

$$\mathcal{R}_A = \frac{|\lambda_2|}{|\lambda_3|}, \quad \mathcal{R}_B = \frac{|\lambda_1|}{\sqrt{|\lambda_2\lambda_3|}} \quad (2)$$

$$\mathcal{S} = \|\mathcal{H}_\sigma\|_F = \sqrt{\sum_j \lambda_j^2} \quad j=1,2,3 \quad (3)$$

This vesselness filter can be interpreted as mapping second order features into probability-like estimates of vessel likeliness. For an ideal tubular structure, it is expected that \mathcal{R}_A is one, and \mathcal{R}_B is small. The measure \mathcal{S} corresponds to the degree of (2nd order) image structureness. The parameters α , β and c tune the sensitivity of the filter to deviations in \mathcal{R}_A , \mathcal{R}_B and \mathcal{S} relative to the ideal behavior for a line structure. The second order derivatives to construct the Hessian matrix are computed using normalized scaled Gaussian derivatives. The filter is applied at multiple scales and the maximum response across scales is selected to ensure that the method is sensitive to a range of vessel widths. Furthermore, the scale at which the output is maximum gives a rough indication of the vessel width, while the eigenvectors give information of the orientation of the vessel segment. Based on the vesselness discriminant function, and user-initialized start and end points, the central vessel axis can be found, *e.g.* by fitting a spline using energy minimization [10] or by using a minimum cost path approach using a discrete [17] or continuous approach [18].

Upon constructing the central vessel axis, the second step of the procedure is either (i) utilizing this axis for visualization [14] or direct quantitative measurements, or (ii) utilizing this axis as initialization for segmentation algorithms [10, 11, 15]. In Fig. 1 an example of the use of

the central vessel axis for improved coronary visualization is shown. Normally, in order to view a large coronary segment multiple slices have to be examined. By first determining the central coronary axis, a multiplanar reformat can be made which visualizes the entire coronary in a single plane [13].

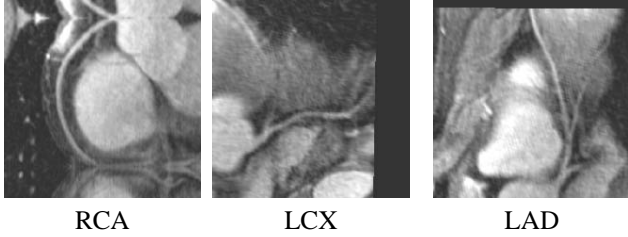


Fig. 1. Automatically extracted central coronary axis is used to visualize coronaries in a single plane using multiplanar reformatting

For vessel segmentation based on the central vessel axis, a number of different approaches can be utilized. In one approach [10, 11] a NURBS surface is initialized along the central vessel axis and attracted to the boundary using a feature image that incorporates knowledge of the image formation process. Another approach [15] utilizes the central vessel axis as initialization for level-set based segmentation. Fig. 2 shows results of these methods in carotid artery segmentation for stenosis grading. In an evaluation study it was found that the automated methods performed better than inter-observer variability [11].

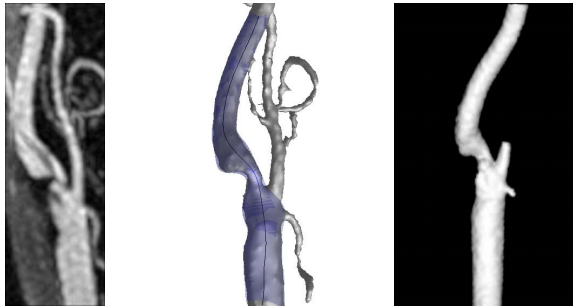


Fig. 2. Maximum intensity projection of carotid artery (left) and segmentations obtained using a NURBS surface (middle) and level set segmentation (right).

3. CARDIAC SEGMENTATION

In the overview of model-based cardiac segmentation [3] ASM models were indicated as a promising approach [19]. The underlying idea of AMSs [20] is that prior knowledge is learned from the variability of shapes observed in a training

set. One major drawback of this method is that in the construction of the model a large collection of corresponding landmark sets between shapes in the training set needs to be established. Manual identification of corresponding landmarks is a time-consuming and tedious task, especially in 3D. Several authors have proposed automatic procedures for finding corresponding landmark points based on segmented images [20-23]. We have utilized an approach [25] in which corresponding landmarks are obtained by mapping the landmarks of an atlas that is representative of the shapes in the training set to individual instances of the training set (see Fig. 3).

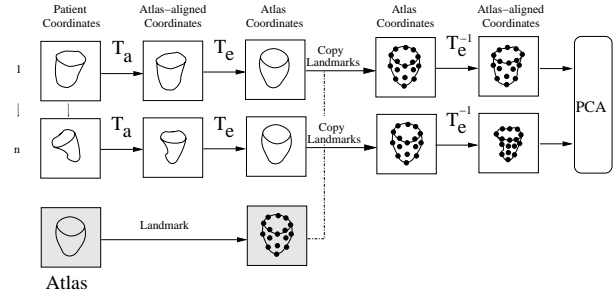


Fig. 3. Construction of a heart model. Landmarks of an atlas are propagated to all other shapes of the atlas using a quasi-affine registration and an elastic registration. PCA analysis in an atlas-aligned coordinate system is used to construct the heart point distribution model.

Given a landmarked average shape or atlas, the landmarks are warped to the individual shapes in the training set by a transformation $T = T_a + T_e$. Here T_a is a quasi-affine registration to map the shape into atlas-aligned coordinates and T_e is an elastic deformation. The elastic deformation is a multi-resolution volumetric free-form deformation that is computed using the method proposed by Rueckert et al. [26]. Once the global transformation T has been applied, the landmarks can be copied from the atlas to the individual shape and the inverse transformation T_e^{-1} can be applied to obtain the landmark positions in the atlas-aligned coordinate system. This process is performed for each shape in the training set. As a result, a set of landmarked shapes is obtained that represents shape differences with respect to the atlas. Since all shapes are in atlas-aligned coordinates, pose and size variations are eliminated from further analysis.

Once the corresponding landmarks have been found, the resulting sets of points can be used to determine a statistical shape model. First, all shapes are described by a 3-dimensional vector \mathbf{x} , where n is the number of landmarks. The model is now described by the mean shape:

$$\bar{\mathbf{x}} = \frac{1}{N} \sum_{i=1}^N \mathbf{x}_i \quad (4)$$

and a matrix Φ which contains the t eigenvectors corresponding to the largest eigenvalues of the covariance matrix

$$S = \frac{1}{N-1} \sum_{i=1}^N (x_i - \bar{x})(x_i - \bar{x})^T \quad (5)$$

Any shape in the training set can now be approximated by

$$x \approx \bar{x} + \Phi b \quad (6)$$

where

$$b = \Phi^T(x - \bar{x}) \quad (7)$$

Shapes similar to those seen in the training set can be generated by varying x according to (6) while applying limits to the parameters b_i , e.g. $\pm 3\sqrt{\lambda_i}$. The number of eigenvectors contained in Φ is chosen in such a way that a predefined proportion of the variance present in the data can be described by the model. In Fig. 4 an example of a heart model built out of fourteen segmented datasets is shown.

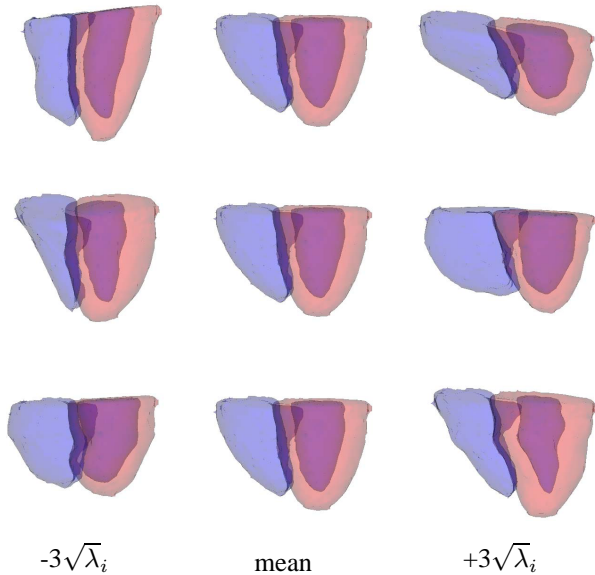


Fig. 4. Shape instances of the 3D cardiac model.

In order to test how well the model built with the automatic landmarking method generalises, a leave-one-out experiment has been performed in which a single shape is approximated by the model built from the remaining shapes. If the training set does not contain all the variation that is expected to occur within the family of shapes, significant errors will be introduced. Therefore the experiment is carried out for a small (15), medium (50) and large (100) set of training shapes. In Fig. 5 both the cumulative variance and the reconstruction error are plotted as a function of the number of modes for the three models. It can be observed that

the ASM approach achieves a compact model (few modes are needed to explain the variance) even if a large training set is used. Also, a larger training set yields an improved model as the reconstruction error for a given number of modes is smaller.

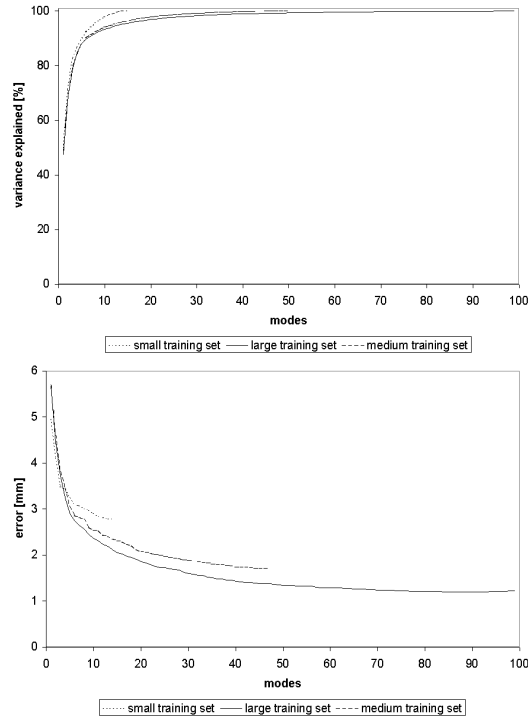


Fig. 5. Graphs displaying the variance that is explained as a function of the number of modes (top) and the reconstruction error in a leave-one-out experiment (bottom) where the individual shapes are fitted with the model of the remaining shapes.

4. SUMMARY

A brief overview of our work in model-based segmentation of cardiac and vascular images is presented. In our experience, for vascular image analysis a simple model based on an automatically extracted central vessel axis is useful in a wide range of applications. For cardiac segmentation, ASMs provide a powerful framework, and an approach is presented to automatically construct point distribution models from segmented shapes for this purpose.

5. REFERENCES

- [1] T. McInerney and D. Terzopoulos, “Deformable models in medical image analysis: a survey,” *Medical Image Analysis*, vol. 1, no. 2, pp. 91–108, 1996.

- [2] A. Singh, D. Goldgof, and D. Terzopoulos, *Deformable models in medical image analysis*, IEEE Computer Society Press, 1998.
- [3] A. Frangi, W. J. Niessen, and M. A. Viergever, "Three-dimensional modeling for functional analysis of cardiac images," *IEEE Trans. Med. Im.*, vol. 20, no. 1, pp. 2–25, 2001.
- [4] H. E. Cline, D. R. Thedens, P. Irazzaval, C. H. Meyer, B. S. Hu, D. G. Nishimura, and S. Ludke, "3D MR coronary artery segmentation," *Magnetic Resonance in Medicine*, vol. 40, no. 5, pp. 697–702, 1998.
- [5] Y. Sato, S. Nakajima, N. Shiraga, H. Atsumi, S. Yoshida, T. Koller, G. Gerig, and R. Kikinis, "Three-dimensional multi-scale line filter for segmentation and visualization of curvilinear structures in medical images," *Medical Image Analysis*, vol. 2, no. 2, pp. 143–168, 1998.
- [6] D.L. Wilson and J. A. Noble, "An adaptive segmentation algorithm for time-of-flight MRA data," *IEEE Trans. Med. Im.*, vol. 18, no. 10, pp. 938–945, 1999.
- [7] E. Bullitt, S. Aylward, K. Smith, S. Mukherji, M. Jiroutek, and K. Muller, "Symbolic description of intracerebral vessels segmented from magnetic resonance angiograms and evaluation by comparison with X-ray angiograms," *Medical Image Analysis*, vol. 5, no. 2, pp. 157–169, 2001.
- [8] L. M. Lorigo, O. D. Faugeras, W. E. L. Grimson, R. Keriven, R. Kikinis, and C. Navabi, A. Westin, "CURVES: Curve evolution for vessel segmentation," *Medical Image Analysis*, vol. 5, no. 3, pp. 195–206, 2001.
- [9] P. J. Yim, J. J. Cebra, R. Mullick, H. B. Marcos, and P. L. Choyke, "Vessel surface reconstruction with a tubular deformable model," *IEEE Trans. Med. Im.*, vol. 20, no. 12, pp. 1411–1421, 2001.
- [10] A. Frangi, W. J. Niessen, R.M. Hoogeveen, Th. Van Walsum, and M. A. Viergever, "Model-based quantitation of 3-D magnetic resonance angiographic images," *IEEE Trans. Med. Im.*, vol. 18, no. 10, pp. 946–956, 1999.
- [11] A. Frangi, W. J. Niessen, P. J. Nederkoorn, J. Bakker, W. P. Th. M. Mali, and M. A. Viergever, "Quantitative analysis of vascular morphology from 3D MR angiograms: in vitro and in vivo results," *Magnetic Resonance in Medicine*, vol. 45, no. 2, pp. 311–322, 2001.
- [12] O. Wink, W. J. Niessen, and M. A. Viergever, "Fast delineation and visualization of vessels in 3D angiographic images," *IEEE Trans. Med. Im.*, vol. 19, no. 4, pp. 337–346, 2000.
- [13] O. Wink, W. J. Niessen, A. F. Frangi, B. Verdonck, and M. A. Viergever, "3D MRA coronary axis determination using a minimum cost path approach," *Magnetic Resonance in Medicine*, 2002, In press.
- [14] C. M. van Bommel, W. J. Niessen, O. Wink, B. Verdonck, and M. A. Viergever, "Blood pool agent CE-MRA: improved arterial visualization of the aortoiliac vasculature in the steady-state using first-pass data," in *MICCAI*, 2001, pp. 699–706.
- [15] C. M. van Bommel, L. Spreeuwers, B. Verdonck, M. A. Viergever, and W. J. Niessen, "Blood pool agent CE-MRA: improved arterial visualization of the aortoiliac vasculature in the steady-state using first-pass data," in *SPIE Medical Imaging*, 2002, In Press.
- [16] A. Frangi, W. J. Niessen, K. L. Vincken, and M. A. Viergever, "Multiscale vessel enhancement filtering," in *Medical Image Conference and Computer Assisted Interventions*, 1998, pp. 130–137.
- [17] E. W. Dijkstra, "A note on two problems in connexion with graphs," *Numerische Mathematik*, vol. 1, pp. 269–271, 1959.
- [18] J. A. Sethian, *Level set methods and fast marching methods: evolving interfaces in computational geometry, fluid mechanics, computer vision and material sciences*, Cambridge Univ. Press, 1999.
- [19] S.C. Mitchell, B.P.F. Lelieveldt, R.J. van der Geest, H.G. Bosch, J.H.C. Reiber, and M. Sonka, "Multistage hybrid active appearance model matching: segmentation of left and right ventricles in cardiac MR images," *IEEE Trans. Med. Im.*, vol. 8, pp. 415–423, 2001.
- [20] T.F. Cootes, C.J. Taylor, D.H. Cooper, and J. Graham, "Active shape models - their training and application," *Computer Vision and Image Understanding*, vol. 61, no. 1, pp. 38–59, 1995.
- [21] A. Kelemen, G. Székely, and G. Gerig, "Elastic model-based segmentation of 3-d neuroradiological data sets," *IEEE Trans. Med. Im.*, vol. 18, no. 10, pp. 828–839, 1999.
- [22] A.D. Brett and C.J. Taylor, "A method of automated landmark generation for automated 3D PDM construction," *Image and Vision Computing*, vol. 18, no. 9, pp. 739–748, 2000.
- [23] M. Fleute and S. Lavalée, "Incorporating a statistically based shape model into a system for computer-assisted anterior cruciate ligament surgery," *Medical Image Analysis*, vol. 3, no. 3, pp. 209–222, 1999.
- [24] M. Kaus, V. Pekar, C. Lorenz, R. Truyen, S. Lobregt, J. Richolt, and J. Weese, "Automated 3D pdm construction using deformable models," in *International Conference on Computer Vision*, 2001, pp. 566–572.
- [25] A. F. Frangi, D. Rueckert, J. A. Schnabel, and W. J. Niessen, "Automatic 3D pdm construction via atlas-based landmarking and volumetric elastic registration," *Information Processing in Medical Imaging*, pp. 78–91, 2001.
- [26] D. Rueckert, L.I. Sonoda, C. Hayes, D.L.G. Hill, M.O. Leach, and D.J. Hawkes, "Nonrigid registration using free-form deformations: application to breast mr images," *IEEE Trans. Med. Im.*, vol. 18, no. 8, pp. 712–721, 1999.